CONFERENCES AND SYMPOSIA

Exotic Lifshitz transitions in topological materials

Physics – Uspekhi **61** (1) 89 – 98 (2018)

CONFERENCES AND SYMPOSIA

PACS numbers: **04.70. – s**, **71.30. + h**, **73.22. – f**

THE 100th ANNIVERSARY OF THE BIRTH OF I M LIFSHITZ

Exotic Lifshitz transitions in topological materials

G E Volovik

DOI: https://doi.org/10.3367/UFNe.2017.01.038218

Contents

Abstract. Topological Lifshitz transitions involve many types of topological structures in momentum and frequency–momentum spaces, such as Fermi surfaces, Dirac lines, Dirac and Weyl points, etc., each of which has its own stability-supporting topological invariant (N_1, N_2, N_3, $\tilde{N}_3$, etc.). The topology of the shape of Fermi surfaces and Dirac lines and the interconnection of objects of different dimensionalities produce a variety of Lifshitz transition classes. Lifshitz transitions have important implications for many areas of physics. To give examples, transition-related singularities can increase the superconducting transition temperature; Lifshitz transitions are the possible origin of the small masses of elementary particles in our Universe, and a black hole horizon serves as the surface of the Lifshitz transition between vacua with type-I and type-II Weyl points.

Keywords: topological Lifshitz transitions, Fermi surface, Dirac point, Weyl point, black hole event horizon

G E Volovik Low Temperature Laboratory, Aalto University, P.O. Box 15100, FI-00076 Aalto, Finland;
Landau Institute for Theoretical Physics, Russian Academy of Sciences, ul. Kosygina 2, 119334 Moscow, Russian Federation;
Lebedev Physical Institute, Russian Academy of Sciences, Leninskii prosp. 53, 119991 Moscow, Russian Federation
E-mail: volovik@ltl.tkk.fi, volovik@itp.ac.ru

Received 29 August 2017
Uspekhi Fizicheskikh Nauk **188** (1) 95 – 105 (2018)
DOI: https://doi.org/10.3367/UFNr.2017.01.038218
Translated by G E Volovik; edited by A Radzig

1. Introduction. Fermi surface, Dirac line, Weyl point

The key word in considering Lifshitz transitions is topology. Following original Lifshitz paper [1], the Lifshitz transition was viewed as a change in the topology of the Fermi surface without symmetry breaking. Later on, it became clear that the topology of the shape is not the only topological characterization of the Fermi surface. The Fermi surface itself represents the singularity in the Green's function G, which is topologically protected: it is the vortex line in the four-dimensional frequency–momentum space in Fig. 1a. The stability of the Fermi surface under interaction between fermions constitutes the origin of the Fermi-liquid theory developed by Landau. Moreover, the Fermi surface appeared to be only one in the series of topologically stable singularities [2, 3], which include, in particular, the Weyl point — the hedgehog in momentum space in Fig. 1b, and the Dirac line — the vortex line in the three-dimensional momentum space in Fig. 1c. The stability of these objects is supported by the corresponding topological invariants in momentum space or in extended frequency–momentum space.

The combination of topology of the shape of the Fermi surfaces, Fermi lines, and Fermi points, together with the topology, which supports the stability of these objects, as well as the topology of the interconnections of objects of different dimensions, provides a large number of different types of Lifshitz transitions. Examples of Lifshitz transitions coming from the interplay of different topological objects in momentum space are discussed in Refs [4–6] and in Sections 3.3 and 4. This makes the Lifshitz transitions ubiquitous, with applications in high-energy physics, cosmology, black hole physics, and the search for room-T_c superconductivity.

Notably, the Lifshitz transition may give the solution to the hierarchy problem in particle physics: why the masses of

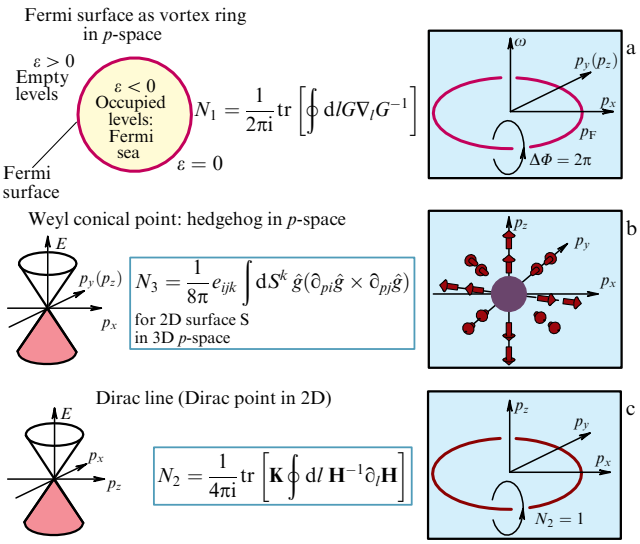

Figure 1. Topologically stable nodes in the energy spectrum of electrons in metals or fermions in general case. (a) Fermi surface represents the singularity in the Green's function, which forms the vortex in the $3+1$ $(\mathbf{p},\omega)$-space, see Section 2.1 and Fig. 2 (in the $2+1$ (p_x,p_y,ω)-space, this is the vortex line). The stability of the vortex is supported by the winding number — the integer-valued invariant N_1, expressed in terms of the Green's function. Lifshitz transitions, which involve the Fermi surfaces, are discussed in Sections 2 and 4. (b) Conical point in the fermionic spectrum of Weyl materials (Weyl semimetals, chiral superfluid ^{3}He-A, and the vacuum of the Standard Model in its gapless phase; see Section 3 and Fig. 9). The directions of spin (or of the emergent spin, isospin, pseudo-spin, etc.) form the topological object in momentum space — the hedgehog or the Berry phase monopole [7] — described by the integer-valued topological invariant N_3. Lifshitz transitions, which involve Weyl nodes, are discussed in Sections 3, 4, and 6. (c) Dirac lines — lines of zeroes in the energy spectrum, described by the topological invariant N_2. The circular line is the Dirac line in the quasiparticle spectrum in the polar phase of superfluid ^{3}He, which has been recently created in aerogel [8]. The same invariant N_2 stabilizes the point nodes in the spectra of 2D materials, such as graphene (see Section 5).

elementary particles in our Universe are so extremely small compared with the characteristic Planck energy scale. Indeed, when we compare the mass $\sim 10^2$ GeV of the most heavy particle — the top quark — with the Planck energy $\sim 10^{19}$ GeV, we can see that the vacuum in our Universe is practically gapless. There are several topological scenarios which may lead to the (almost) gapless vacuum.

In one scenario, the quantum vacuum belongs to the class of gapless (massless) Weyl materials in Fig. 1b, where the nodes in the spectrum of elementary particles — the Weyl points — are topologically protected [2, 3, 9] (see Section 3.1 and Fig. 9). According to this scenario, the physical laws are not fundamental, but emerge in the low-energy corner of the quantum vacuum, i.e., in the vicinity of the Weyl points, where the spectrum becomes linear and all the symmetries of the Standard Model, including Lorentz invariance and general covariance, emerge from nothing. In this scenario, the Lifshitz transition between type-I and type-II Weyl vacua takes place at the black hole horizon (see Section 3.4).

At an even lower energy, some of these symmetries experience spontaneous breaking, analogous to the superconducting transition, in which the hierarchy problem is understood: in most superconductors, the transition temperature T_c is exponentially small compared to the characteristic Fermi energy scale (an analog of the Planck scale), which forces us to search for exceptional materials with enhanced T_c. The role of the Lifshitz transition in the elevation of the superconducting transition temperature is discussed in Sections 2.4 and 3.3.

In the other scenario, the massless (gapless) vacua emerge at the Lifshitz transition between the fully gapped vacua with various topological charges (see Section 6 and Fig. 18). The almost perfect masslessness of elementary particles in our Universe suggests that the Universe is very close to the line of the topological Lifshitz transition between fully gapped vacua, at which fermions necessarily become gapless [10] (see Section 6). This is the topological analog of the so-called multiple point principle, according to which the Universe lives in the coexistence point (line, surface, etc.) of the first-order phase transition, where different vacua have the same energy [11–15].

2. Fermi surface and Lifshitz transitions

2.1 Fermi surface as topological object

The primary topology, which is at the origin of Lifshitz transitions, is the one which is responsible for the stability of the Fermi surface itself. If the Fermi surface is not stable under electron–electron interactions, the consideration of the topology of the shape of the Fermi surface and of the corresponding Lifshitz transitions does not make much sense. To view the topological stability of the Fermi surface with respect to interactions, let us start with the Green's function of an ideal Fermi gas in Fig. 2a. The Fermi surface $\varepsilon(\mathbf{p}) = 0$ of the noninteracting Fermi gas is the boundary in a momentum space, which separates the occupied states with $\varepsilon(\mathbf{p}) < 0$ from the empty states with $\varepsilon(\mathbf{p}) > 0$. The Green's function $G(\omega,\mathbf{p})$ with ω on imaginary axis, viz.

$$G^{-1}(\omega,\mathbf{p}) = i\omega - \varepsilon(\mathbf{p})\,, \tag{1}$$

has a singularity at $\omega = 0$ and $\varepsilon(\mathbf{p}) = 0$. In Fig. 2b, the p_z coordinate is dropped for clearness, and the Green's function singularity forms the closed line in the $2+1$ momentum–frequency space (p_x,p_y,ω). This line represents the vortex

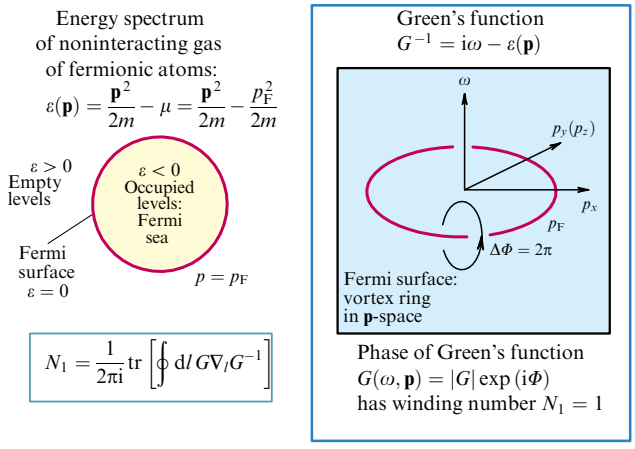

Figure 2. Fermi surface is robust to interactions, because it represents the topologically stable singularity in the Green's function — the vortex in the $3+1$ $(\mathbf{p},\omega)$-space. The stability of the vortex is supported by the winding number of the phase Φ of the Green's function $G = |G|\exp(i\Phi)$. In general, the winding number is given by the integer-valued invariant N_1, expressed in terms of the Green's function, see Eqn (2).

line, in which the phase $\Phi(p_x, p_y, \omega)$ of the Green's function has the 2π winding. As in the case of the real-space vortex in superfluids, the integer winding number provides the stability of the Fermi surface with respect to perturbations, including the interaction [if the p_z component is restored, the singularity forms the vortex sheet in the $3+1$ momentum–frequency $(\mathbf{p}, \omega)$ space].

In general, when the Green's function has the spin, band, and other indices, the winding number can be written in terms of the Green's function as the following topological invariant

$$N_1 = \mathrm{tr} \oint_C \frac{\mathrm{d}l}{2\pi \mathrm{i}} \, G(\omega, \mathbf{p}) \, \partial_l G^{-1}(\omega, \mathbf{p}) \,. \tag{2}$$

Here, the integral is taken over an arbitrary contour C around the momentum–frequency vortex sheet, and tr stands for the trace over all the indices.

Due to topological stability, one cannot make a hole in the Fermi surface. As in the case of vortex lines, which cannot terminate in a bulk, the Fermi surface has no edges.

2.2 Fermi surface and Lifshitz transitions

Because of topological stability, a Fermi surface may be formed even in the superconducting state. The conditions for that are a multiband structure, symmetry breaking with respect to time T reversal and parity P [16–20]. These so-called Bogoliubov Fermi surfaces also appear in gapless superfluids, when the Weyl points in ^{3}He-A and the Dirac nodal line in the polar phase of ^{3}He are inflated to Fermi pockets in the presence of superflow, which violates both T and P symmetries [21, 22].

The Fermi surface can also be formed in fully gapped superfluids if the velocity of superflow exceeds the Landau critical velocity [3, 23]. Exceeding the Landau velocity with the formation of closed Bogoliubov Fermi surfaces is an example of one of the two transitions suggested by Lifshitz (Fig. 3).

Another original Lifshitz transition takes place when the Fermi surface crosses the stationary point of the electronic energy spectrum. Near the transition, the expansion of the generic spectrum has the form [1]

$$\varepsilon_{\mathbf{p}} = a p_x^2 + b p_y^2 + c p_z^2 - \mu \,. \tag{3}$$

For $a > 0$, $b > 0$, $c < 0$, the transition with disruption of the neck of the Fermi surface at $\mu = 0$ is shown in Fig. 4a. In terms of the vortex singularities of the Green's function in a $3+1$ $(\mathbf{p}, \omega)$ space, this Lifshitz transition represents the interconnection of the vortex lines in Fig. 4b. In superfluids, the interconnection of the real-space vortices exhibits an important process in the vortex turbulence [24].

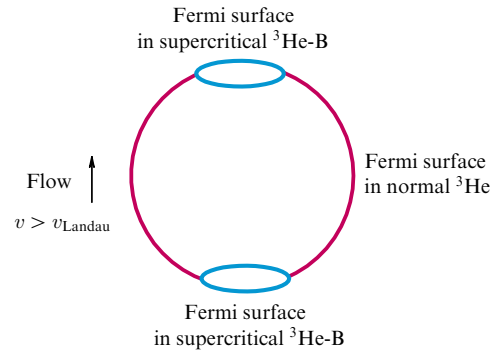

Figure 3. Lifshitz transition in which the closed Fermi surfaces (pockets) appear in the fully gapped superfluid ^{3}He-B, when the flow velocity of the liquid with respect to the walls of the container exceeds the Landau critical velocity [3, 23].

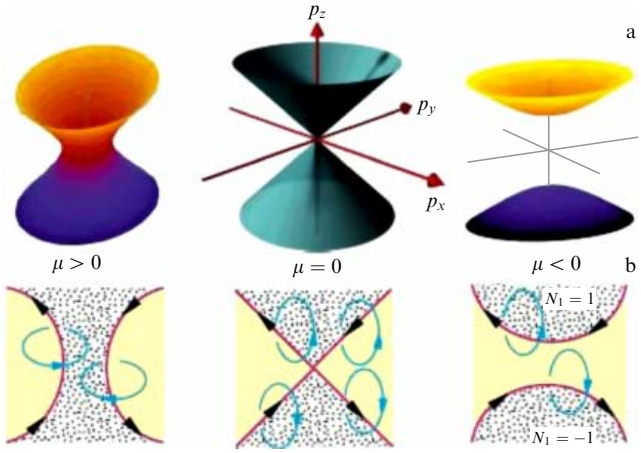

Figure 4. Since the Fermi surface represents the vortex in a $3+1$ $(\mathbf{p}, \omega)$ space, the Lifshitz transition with disruption of the neck of the Fermi surface [1] (a) is equivalent to the interconnection of vortices in quantum turbulence [24] (b).

2.3 From pole of Green's function to zero

While in a conventional Landau Fermi liquid the Green's function has a pole, for a Luttinger liquid the residue of the pole in the Green's function has a singularity — the parameter γ in Eqn (5) is nonzero [25]:

$$G = \frac{Z}{\mathrm{i}\omega - \varepsilon(\mathbf{p})} \,, \qquad Z \propto \left(\omega^2 + \varepsilon^2(\mathbf{p})\right)^{\gamma} . \tag{4}$$

Nevertheless, the topological invariant remains the same for all γ, i.e., the Green's function has the same topological property as the Green's function of a conventional metal with a Fermi surface at $\varepsilon(\mathbf{p}) = 0$. This is the reason why the Luttinger theorem is still valid [26, 27]. The particle number density of interacting fermions is equal to the volume in the momentum space enclosed by a singular surface with the topological charge $N_1 = 1$, irrespective of the realization of the singularity.

The suppression of residue Z can be so strong that the pole in the Green's function is transformed to the zero of the Green's function, which corresponds to the special case of $\gamma = 1$ (Fig. 5):

$$G \propto \mathrm{i}\omega + \varepsilon(\mathbf{p}) \,. \tag{5}$$

This situation in particular takes place for Mott insulators [26], which means that the topology of the Fermi surface is preserved even in the insulating phase, and thus the Luttinger theorem is still valid [26, 27]. Thus, it may be argued that the transition between metals and insulators can also be viewed as a type of zero-temperature Lifshitz transition, in which the property of the energy spectrum drastically changes without symmetry breaking. However, this quantum phase transition is not topological, since the topological invariant does not change across the transition.

It cannot be ruled out that in the so-called pseudogap phase of cuprate superconductors and some other materials

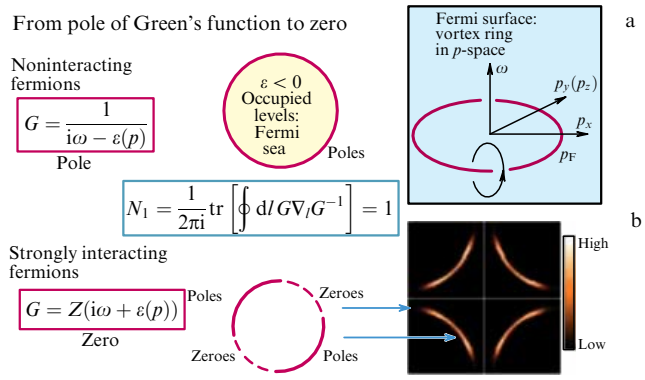

Figure 5. Lifshitz transition in which the whole Fermi surface of the poles in the Green's function or part of the Fermi surface transforms into a surface of zeroes in the Green's function. The topological charge of the surface does not change at this quantum phase transition. As a result, the Luttinger theorem remains valid [26, 27], i.e., the particle number density of interacting fermions is equal to the volume in the momentum space enclosed by a singular surface with the topological charge $N_1 = 1$.

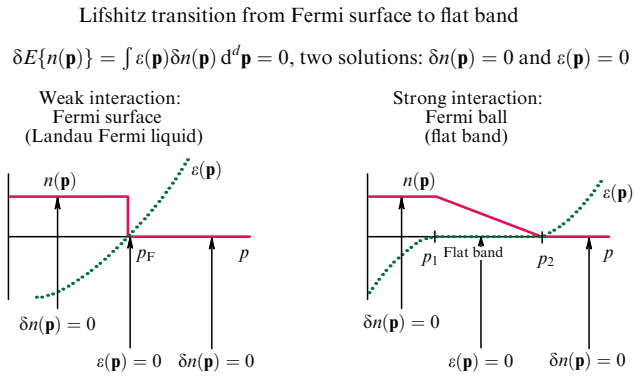

Figure 6. Formation of a flat band in a system of strongly interacting fermions in the Landau theory approach. There are two types of extrema of the energy functional $E\{n(\mathbf{p})\}$: (i) $\delta n(\mathbf{p}) = 0$, which corresponds to the occupied $n(\mathbf{p}) = 1$ and free $n(\mathbf{p}) = 0$ levels; (ii) $\varepsilon(\mathbf{p}) = 0$, this solution takes place when $0 < n(\mathbf{p}) < 1$. On the weak interaction side, solution (i) takes place inside and outside the Fermi surface, while solution (ii) corresponds to the Fermi surface itself. On the strong interaction side, the solution $\varepsilon(\mathbf{p}) = 0$ is extended to the 3D band — the flat band. Formation of the flat band from the Fermi surface occurs via a new type of Lifshitz transition.

(see, e.g., Ref. [28]) a part of the Fermi surface transforms into a surface of zeroes in the Green's function and Fermi arcs are formed (see right-hand panel in Fig. 5b).

2.4 From Fermi surface to flat band

The flat band — or the so-called Khodel–Shaginyan fermion condensate, where all the states have zero energy — is caused by electron–electron interactions [29–31]. This is a manifestation of the general phenomenon of merging the energy levels due to interactions (Fig. 6). Such an effect has been observed for Landau levels in 2D quantum wells [32, 33]. Since the flat band has a huge density of electronic states, this may considerably elevate the transition temperature to the superconducting state (Fig. 7).

The flat band is more easily formed in the vicinity of the conventional Lifshitz transition [34, 35] (Fig. 8). Flattening of the single-particle spectrum near the Fermi momentum has been reported in a 2D quantum well [36]. It is possible that

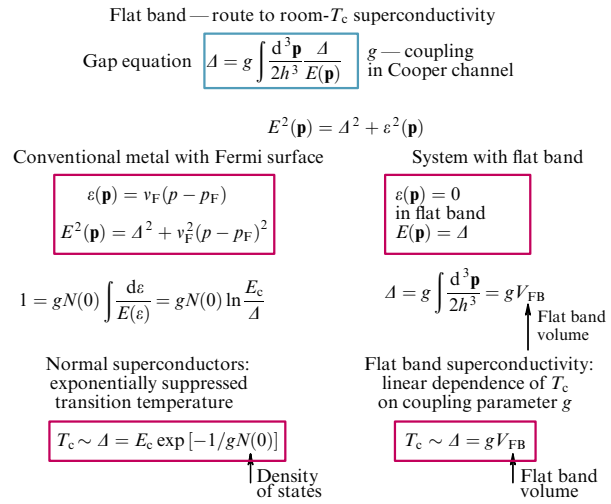

Figure 7. Flat band of electronic states with zero energy leads to the linear dependence of transition temperature T_c on the coupling parameter [29], while in conventional metals T_c is exponentially suppressed.

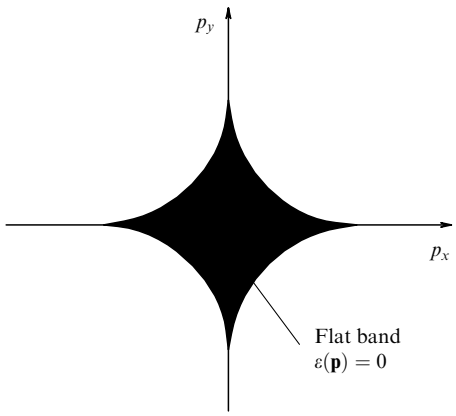

Figure 8. Flat band emerging in the vicinity of the Lifshitz transition in Fig. 4 due to electron–electron interactions [34, 35]. The original noninteracting spectrum is $\varepsilon^{(0)}(\mathbf{p}) = p_x p_y/m - \mu$, where the Lifshitz transition takes place at $\mu = 0$. Due to the interaction, all the states in the black region have zero energy (the flat band is shown at the point of the Lifshitz transition).

this effect is responsible for the occurrence of superconductivity with high T_c observed in pressurized sulfur hydride [37, 38]: there is some theoretical evidence that high-T_c superconductivity takes place at such a pressure when the system is close to the Lifshitz transition [39–41]. Enhanced superconductivity at the Lifshitz transition has been reported for an FeSe monolayer [42].

3. Lifshitz transitions governed by Weyl point topology

3.1 Topology of Weyl fermions

Weyl particles are the elementary particles of our Universe. The Weyl spinor contains 2 complex components, and these massless particles are described by the 2×2 complex Hamiltonian: $H = c\boldsymbol{\sigma}\mathbf{p}$ for right-handed quarks and leptons, and $H = -c\boldsymbol{\sigma}\mathbf{p}$ for left-handed particles, where c is the speed of light. Their spins in momentum space form the hedgehog

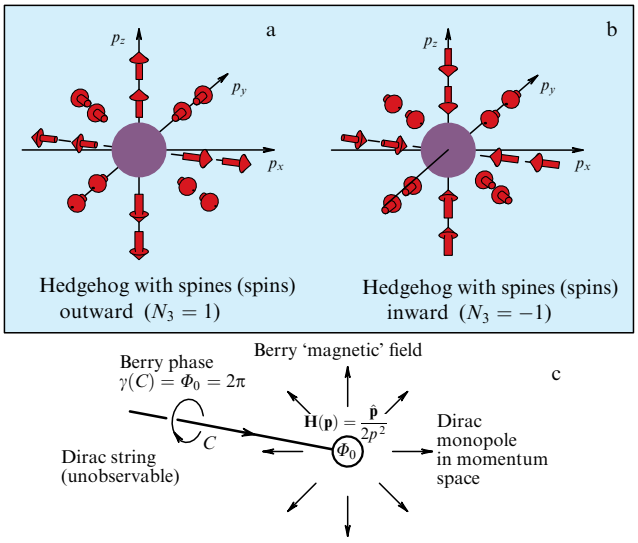

Figure 9. Spins of right-handed Weyl particles (quarks and leptons) are directed along the momentum **p** forming the hedgehog (a). The anti-hedgehog — the hedgehog with spines (spins) inward (b), corresponds to left-handed Weyl particles. (c) The topological invariant N_3 describing the topologically distinct hedgehog configurations is expressed either in terms of the Green's function in Eqn (6) or in terms of the unit vector field in Fig. 1b.

(Fig. 9a) and anti-hedgehog (Fig. 9b), respectively. The hedgehog is a topologically stable object, and thus the Weyl point in the center of the hedgehog is topologically protected. The corresponding topological invariant N_3 for hedgehogs can be expressed in terms of the Green's function as a surface integral in the $3+1$ momentum–frequency space $p_\mu = (\mathbf{p}, \omega)$ [3]:

$$N_3 = \frac{\epsilon_{\mu\nu\rho\sigma}}{24\pi^2}\ \mathrm{tr} \oint_{\Sigma_a} \mathrm{d}S^\sigma\, G\, \frac{\partial}{\partial p_\mu} G^{-1} G\, \frac{\partial}{\partial p_\nu} G^{-1} G\, \frac{\partial}{\partial p_\rho} G^{-1}. \quad (6)$$

Here, Σ_a is a three-dimensional surface around the isolated Weyl point in $(\mathbf{p}, \omega)$ space.

From the point of view of the general properties of the fermionic spectrum, the Weyl point represents the exceptional point of level crossing analyzed by von Neumann and Wigner [43]. Their analysis demonstrated that two branches of a spectrum which have the same symmetry may touch each other at the conical (or diabolical) point in the three-dimensional space of parameters, which in our case are p_x, p_y, and p_z. The touching of two branches is described in general by a 2×2 Hamiltonian $H = \boldsymbol{\sigma}\mathbf{g}(\mathbf{p})$. The topological invariant N_3 is expressed in terms of the unit vector $\hat{\mathbf{g}}(\mathbf{p}) = \mathbf{g}(\mathbf{p})/|\mathbf{g}(\mathbf{p})|$ in Fig. 1b, which forms the hedgehog configuration in Fig. 1b (right). The touching point also represents the Berry phase monopole in Fig. 9c [7]. It cannot be ruled out that the Weyl fermions in the Standard Model (quarks and leptons) are not elementary particles, but emerge from a level crossing at a more fundamental level [2, 3, 9]. In particular, the underlying quantum vacuum may be described by the quantum field theory based on real numbers (Majorana fermions), while the imaginary unit, which enters the Schrödinger equation, emerges in the low-energy limit together with the relativistic linear spectrum of Weyl fermions [44].

The linear ('relativistic') spectrum emerges only for elementary topological charges $N_3 = 1$ or $N_3 = -1$. If the Weyl point has a higher topological charge, $|N_3| > 1$, and if

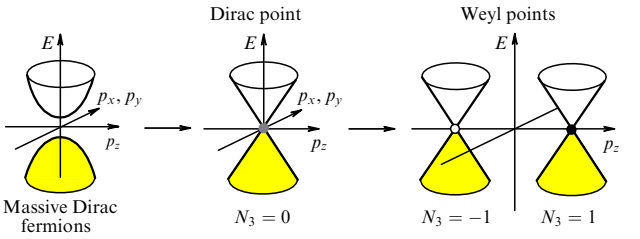

Figure 10. Formation of a pair of Weyl points from the vacuum state with massive Dirac fermions. Topological charges $N_3 = 1$ and $N_3 = -1$ correspond to right-handed and left-handed particles, respectively. At the Lifshitz transition point, the vacuum is gapless, with the Dirac point in the fermionic spectrum, which has topological charge $N_3 = 0$.

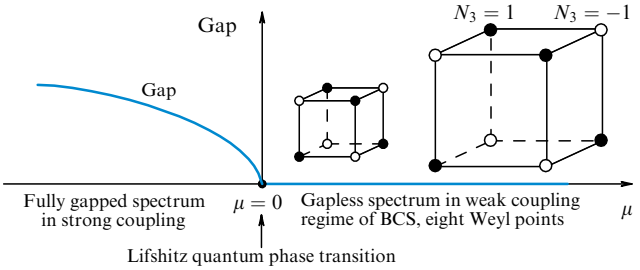

Figure 11. BEC-to-BCS Lifshitz transition with the formation of 4 right-handed and 4 left-handed Weyl points at the vertices of a cube. This arrangement of the Weyl nodes has been discussed for the energy spectrum in superconductors which belong to the $O(D_2)$ symmetry class [47, 48]. In relativistic theories, a similar arrangement gives 8 left and 8 right Weyl fermions on the vertices of a cube in the $3+1$ (p_x, p_y, p_z, ω) space [49, 50].

there is no special symmetry which leads to the degeneracy of the levels, the spectrum possesses different dispersion relations along different axes [3, 45]. For example, at $|N_3| = 2$, the spectrum is 'relativistic' in one direction, and quadratic in the other two directions.

3.2 Lifshitz transitions with splitting of Weyl points

A typical Lifshitz transition, which involves Weyl nodes in the fermionic spectrum, describes the formation of Weyl points with opposite charges $N_3 = \pm 1$ from the fully gapped state. Figure 10 demonstrates the formation of a pair of Weyl points from the vacuum state with massive Dirac fermions. The intermediate state has a massless Dirac point in the fermionic spectrum with the topological charge $N_3 = 0$. Such a gapless Dirac point is marginal but can be protected by symmetry, as takes place in the Standard Model above the electroweak transition. If the symmetry is violated by an external action or is spontaneously broken, the Dirac spectrum either acquires mass or splits into a pair of Weyl points [46].

Figure 11 demonstrates the formation of 4 right-handed and 4 left-handed Weyl points in the Lifshitz transition between the BEC strong coupling regime and the BCS weak coupling regime. Such an arrangement of the Weyl nodes takes place in the energy spectrum in the $O(D_2)$ symmetry class of pair correlated systems [47, 48]. In both cases, the total topological charge $N_3^{\mathrm{total}} = 0$, and thus there is an even number of Weyl fermions, which supports the fermion doubling principle [51]. In relativistic theories, the analogical arrangement of 8 left and 8 right Weyl fermions on the vertices of a cube in the $3+1$ (p_x, p_y, p_z, ω) space has been discussed [49, 50]. It is interesting that each family of

Standard Model fermions contains 8 left and 8 right Weyl particles.

3.3 Lifshitz transition to type-II Weyl cone

There is A type of Lifshitz transition which involves both the Fermi surface (invariant N_1) and the Weyl point (invariant N_3). This is the transition between the isolated Weyl points (type-I Weyl spectrum) and the Weyl point connecting two Fermi surfaces (called the type-II Weyl point [52]). Such transitions have been discussed in Refs [44, 53] in relativistic theories.

The simplest realization of the type-II Weyl point comes from the following Hamiltonian with two parameters c and v:

$$H = c\boldsymbol{\sigma}\mathbf{p} - vp_z\,. \tag{7}$$

At $v = 0$, this is the Weyl point with the Weyl cone in Fig. 12a. For $0 < v < c$, the cone is tilted. For $v > c$, the cone is overtilted, so that the cone crosses the zero energy level forming two Fermi pockets connected by the Weyl point — the type-II Weyl point (Fig. 12b). The Lifshitz transition between two types of Weyl points occurs at $v = c$. It was demonstrated that such a Lifshitz transition also leads to the elevation of the transition temperature to the superconducting state [54, 55] (Fig. 12c).

3.4 Lifshitz transition at the black hole horizon

The Lifshitz transition discussed in Section 3.3 takes place at the black hole horizon. In General Relativity, the stationary metric, which is valid both outside and inside the black hole horizon, is provided, in particular, by the Painlevé–Gullstrand spacetime [57]. The line element of the Painlevé–Gullstrand metric is equivalent to the so-called acoustic metric [58–60]:

$$\mathrm{d}s^2 = g_{\mu\nu}\,\mathrm{d}x^\mu\,\mathrm{d}x^\nu = -c^2\,\mathrm{d}t^2 + (\mathrm{d}\mathbf{r} - \mathbf{v}\,\mathrm{d}t)^2\,. \tag{8}$$

This metric is expressed in terms of the velocity field $\mathbf{v}(\mathbf{r})$ describing frame dragging in the gravitational field:

$$\mathbf{v}(\mathbf{r}) = -\hat{\mathbf{r}}c\sqrt{\frac{r_\mathrm{h}}{r}}\,, \qquad r_\mathrm{h} = \frac{2MG}{c^2}\,. \tag{9}$$

Here, M is the mass of the black hole, r_h is the radius of the horizon, and G is the Newtonian constant of gravitation. Behind the horizon, the drag velocity exceeds the speed of light, $|\mathbf{v}| > c$, and particles are trapped in the hole (see Fig. 13b). The behavior of the light cone (the cone in spacetime) across the event horizon is shown in Fig. 13a. The light cone is overtilted behind the horizon.

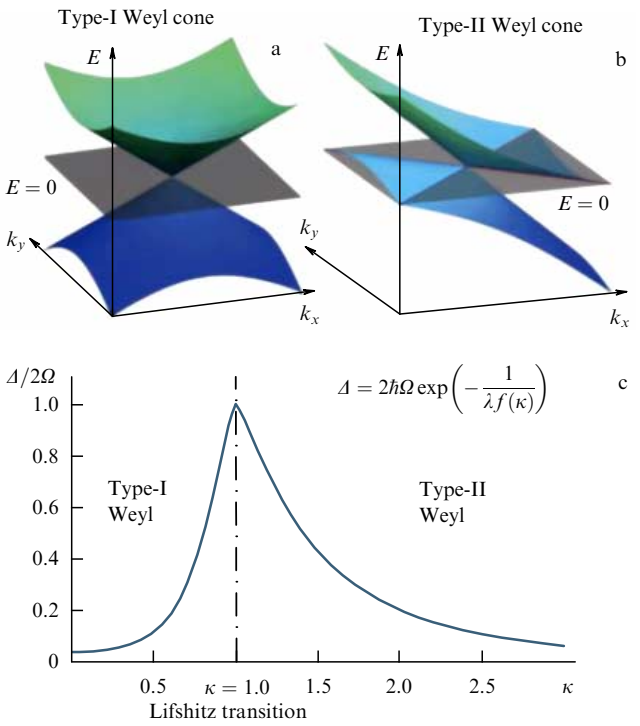

Figure 12. (a) Weyl cone in the spectrum of type-I Weyl fermions. (b) Overtilted Weyl cone in the spectrum of type-II Weyl fermions. (c) Elevation of superconducting transition temperature T_c at the Lifshitz transition between the type-I Weyl and the type-II Weyl points which takes place at $\kappa = 1$, where κ is a parameter of the theory [54].

The behavior of the Weyl cone (the cone in momentum space) across the horizon is described by the Hamiltonian of the Weyl particles in the gravitational field of the black hole, which for the Painlevé–Gullstrand metric has the following form [53]:

$$H = \pm c\boldsymbol{\sigma}\mathbf{p} - p_r v(r)\,, \qquad v(r) = c\sqrt{\frac{r_\mathrm{h}}{r}}\,. \tag{10}$$

Here, the plus and minus signs correspond to the right-handed and left-handed Weyl fermions, respectively, and p_r is the radial component of the linear momentum of the particle. Behind the horizon, where $v > c$ and the light cone is overtilted, the Weyl cone is also overtilted, but in the way shown in Fig. 12. Two Fermi pockets are formed, which touch

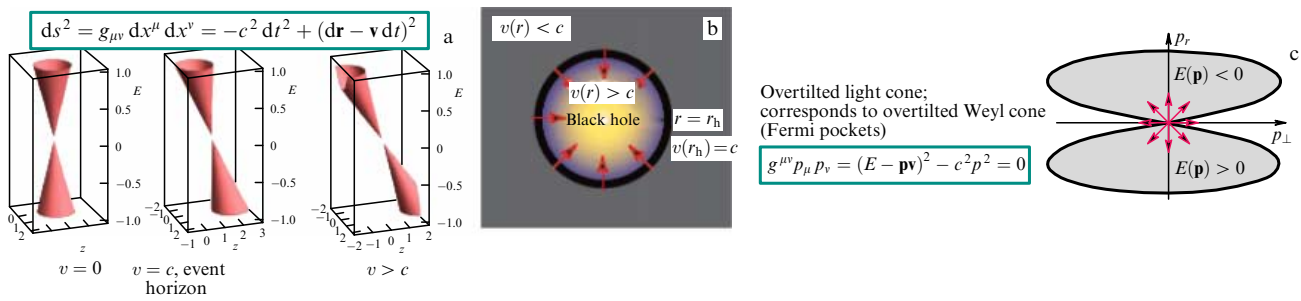

Figure 13. Black hole in the Painlevé–Gullstrand metric. The metric $g_{\mu\nu}$ describes the light cone. The light cone (a) is overtilted behind the horizon, where the frame drag velocity $v > c$ (b). The metric $g^{\mu\nu}$ describes the Weyl cone. The Weyl cone is overtilted behind the horizon, forming two Fermi pockets connected by a type-II Weyl point (c). The horizon at $r = r_\mathrm{h}$ serves as the surface of the Lifshitz transition between the type-I Weyl point for $r > r_\mathrm{h}$ and the type-II Weyl point for $r < r_\mathrm{h}$. This behavior of two cones allows us to simulate the black hole horizon and Hawking radiation using Weyl semimetals [56].

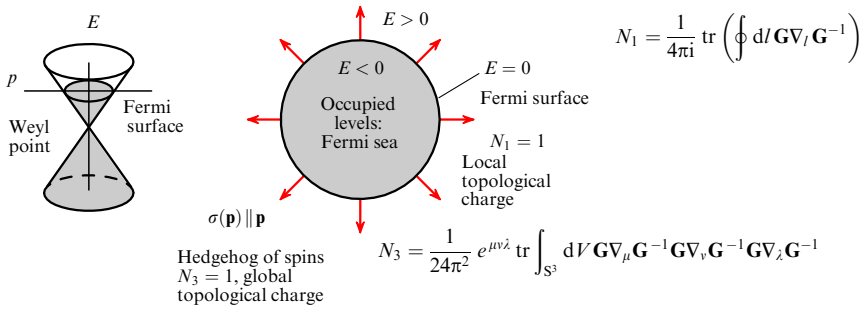

Figure 14. Fermi surface with local topological charge N_1 and the global topological charge N_3 [3]. It contains the Berry phase monopole.

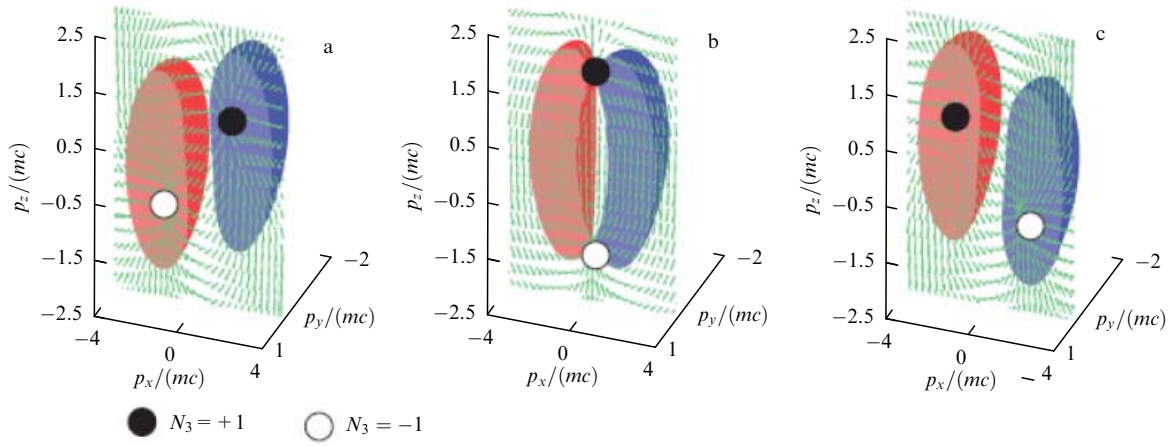

Figure 15. (Color online.) Lifshitz transition with exchange of Berry phase monopoles between two Fermi surfaces [6]. The red and blue Fermi surfaces are globally nontrivial, with $N_3 = -1$ and $N_3 = 1$, respectively. In the process of the Lifshitz transition, two Berry phase monopoles are pushed out from the Fermi surfaces. In the Lifshitz transition, the Fermi surfaces touch each other at the Weyl points, so that the latter become type-II Weyl points. Above the transition, the Weyl points are again inside the Fermi surfaces, but now the red and blue Fermi surfaces have the global charges $N_3 = 1$ and $N_3 = -1$, respectively. The topological charges of Fermi surfaces are transferred between the Fermi surfaces via the type-II Weyl points.

each other at the type-II Weyl point in Fig. 13c). The event horizon at $r = r_h$ thus serves as the surface of the Lifshitz transition.

The correspondence between Weyl semimetals and black holes allows us to simulate the black hole horizon using the inhomogeneous Weyl semimetal, where the transition between the type-I and type-II Weyl points takes place on some surface [60]. This surface would play the role of the event horizon. The formed black hole will be fully stationary in equilibrium. However, just after the creation of this black hole analog, the system is not in the equilibrium state, and the relaxation process at the initial stage of equilibration looks similar to the process of Hawking radiation.

In the discussed Lifshitz transition between type-I and type-II Weyl points, the element g_{00} of the effective metric changes sign. Another type of Lifshitz transition occurs when the element g^{00} changes sign. In Weyl semimetals, this corresponds to the transition to type-III Weyl fermions [61], while in General Relativity this is the transition to spacetimes with closed timelike curves.

4. Lifshitz transitions with several topological charges

In Sections 3.3 and 3.4, we considered the Lifshitz transition, which involved the interaction between two topological charges: the charge N_1, which characterizes the Fermi surface, and the charge N_3 of the Berry phase monopole. There are other Lifshitz transitions with the interplay of these two topological invariants. This happens, in particular, when the closed Fermi surface is described by two invariants: the local charge N_1, which provides the local stability of the Fermi surface, and the global charge N_3, which describes the Weyl point inside the Fermi surface in Fig. 14. The latter takes place, for example, when the Weyl point shifts from the zero energy position forming the small Fermi sphere around the Weyl point (see Fig. 14). This Fermi sphere contains the N_3 charge, which can be obtained from Eqn (6) by integration over the surface, which encloses the Fermi sphere.

In the Lifshitz transition, Fermi surfaces can exchange their global charges N_3 or lose the global charge [6, 46]. An example of exchange is in Fig. 15 and an example of the lost global charge is in Fig. 16. In both cases, the intermediate state at the point of Lifshitz transition contains the type-II Weyl points.

5. Lifshitz transition governed by conservation of N_2 charge

The conical Dirac point in 2D graphene and the nodal lines in 3D semimetals and nodal superfluids and superconductors are stabilized by the topological charge N_2 in Fig. 1c [4, 62]. Dirac nodal lines were known to exist in the polar phase of superfluid ^{3}He [8, 63], in cuprate superconductors, and in graphite (band crossing lines) [64–66]. They are now extensively studied in semimetals [67].

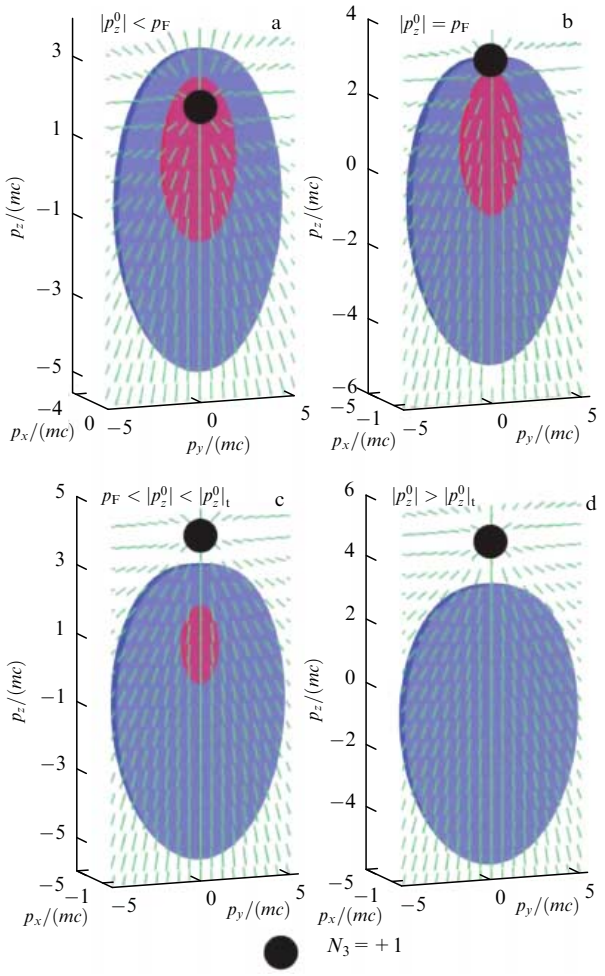

Figure 16. (Color online.) Lifshitz transition in which the Fermi surfaces lose the Weyl charge N_3 [6]. (a) Below the Lifshitz transition point, both surfaces contain the same Berry phase monopole with $N_3 = 1$. (b) At the transition, the Weyl point connects the inner and outer Fermi surfaces. (c) Above the transition, the monopole comes out from the Fermi surfaces, and both Fermi surfaces become globally trivial, with $N_3 = 0$. Without global stability, the Fermi surfaces may shrink and disappear in the conventional Lifshitz transition, as happens with the red Fermi surface in figure (d).

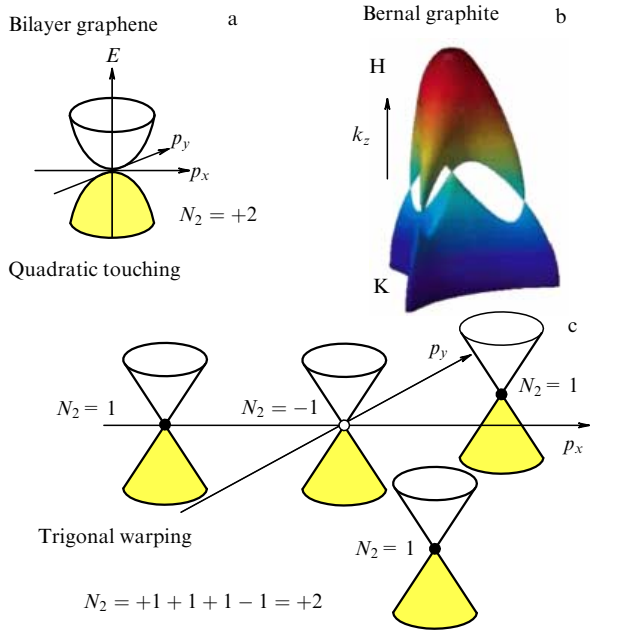

Figure 17. Lifshitz transition governed by conservation of the topological charge N_2 in bilayer graphene, in which two conical points with the same charge $N_2 = 1$ on two graphene layers either merge to form the Dirac point with topological charge $N_2 = 2$ and with a quadratic spectrum (a) or split into four Dirac conical points (c). The latter is called trigonal warping. The total topological charge $N_2 = 2$ in both cases, and thus one configuration may transform into the other one via the Lifshitz transition.

The type of Lifshitz transitions governed by the conservation of the topological charge N_2 is illustrated in Fig. 17 using the example of bilayer graphene, when one graphene layer is shifted with respect to the other one. Merging the two conical points with $N_2 = 1$ leads to the formation of the Dirac node with quadratic dispersion in Fig. 17a, which has the topological charge $N_2 = 2$. This point, in turn, may split into four Dirac conical points with $N_2 = \pm 1$ in Fig. 17c. This is the so-called trigonal warping. The total topological charge is conserved, $N_2 = 1 + 1 + 1 - 1 = 2$. The trigonal warping can be seen in Bernal graphite (see Fig. 17b), and the transition occurs as a function of p_z [64–66], when p_z crosses the so-called nexus point [62, 68].

6. Lifshitz transitions between gapped states via the gapless state

Lifshitz transitions between gapped states include transitions between topological and nontopological insulators; transitions between fully gapped superfluids/superconductors; transitions between 2D systems, which experience the intrinsic quantum Hall effect; etc. Here, we consider this transition using the example of 2D systems, where the Hall conductance is expressed in terms of the integer-valued topological invariant $\tilde{N}_3$ in Fig. 18a [69–72]. This topological invariant has the same structure as the invariant N_3 in Fig. 1b, but the integration is taken now over the whole 2D Brillouin zone. This is an example of dimensional reduction from 3D systems with Weyl nodes to 2D topological insulators [3].

Figure 18a demonstrates the Lifshitz transition between the topological insulator with $\tilde{N}_3 = 1$ and the trivial insulator with $\tilde{N}_3 = 0$. Here, the topological charge is not conserved across the Lifshitz transition, but abruptly changes, resembling the first-order phase transition. Nevertheless, the transition occurs smoothly, because at the point of transition the gap in the energy spectrum vanishes and the topological invariant becomes poorly defined. The nullification of the gap in the transition reflects the fact that in the 3D space (p_x, p_y, μ), where μ is the chemical potential or some other parameter along which the transition occurs, the gap node represents the Weyl point with topological charge $N_3 = \tilde{N}_3(\text{right}) - \tilde{N}_3(\text{left})$ [3, 74].

One example is the 2D $p_x + ip_y$ superfluid/superconductor [73], where the Lifshitz transition between the superfluid states with $\tilde{N}_3 = 1$ and $\tilde{N}_3 = 0$ occurs at the same point $\mu = 0$ as in a normal Fermi liquid. A detailed consideration shows that the Lifshitz transition represents the third-order quantum transition [75]: the third derivative d^3E/dg^3 of the ground state energy E with respect to the interaction strength g is discontinuous. Compare this with the original $2\,1/2$-order transition [1] and the $3\,1/2$-order transition discussed recently [66].

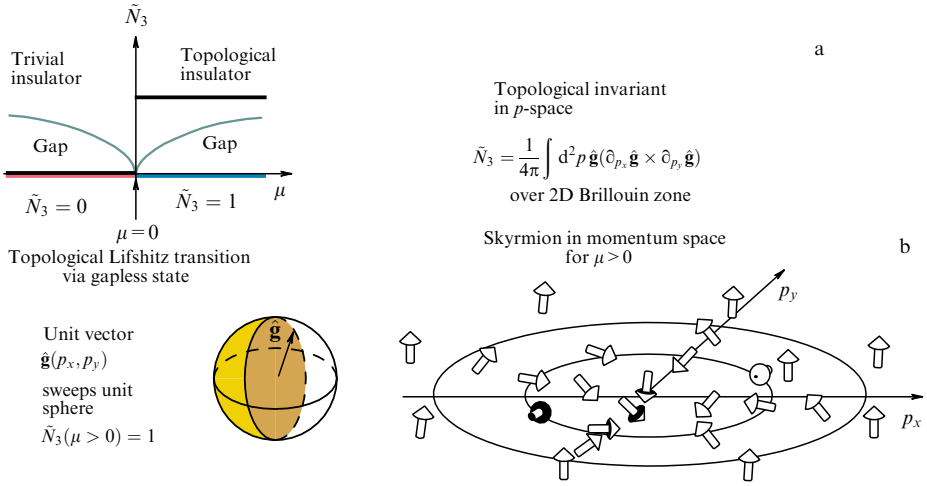

Figure 18. Lifshitz transitions between fully gapped topologically different vacua in 2D systems, which experience the intrinsic quantum Hall effect in the absence of a magnetic field [70–74]. (a) The Hall conductance is expressed in terms of the integer-valued topological invariant $\tilde{N}_3$. The Lifshitz transition between the topological insulator with $\tilde{N}_3 = 1$ and the trivial insulator with $\tilde{N}_3 = 0$ takes place through the state where the gap vanishes (see a left-hand panel of figure a). (b) The topologically nontrivial state with $\tilde{N}_3 = 1$ represents the topologically nontrivial nonsingular object — the skyrmion — in the 2D momentum space.

The nullification of the gap in the fermionic spectrum at the transition between the gapped vacua suggests a scenario for the solution to the hierarchy problem in the particle physics: the relativistic quantum vacuum is almost massless, because our Universe is very close to the line of the Lifshitz transition. The reason why nature would prefer the critical line may be that the gapless states on the phase transition line are able to accommodate more entropy than the gapped states [10].

7. Conclusion

Topological Lifshitz transitions are ubiquitous, since they involve many types of topological structures of the fermionic spectrum: Fermi surfaces, Dirac lines, Dirac and Weyl points, edge states, Majorana zero modes, etc. Each of these structures has their own topological invariant, such as N_1, N_2, N_3, $\tilde{N}_3$, etc., which supports the stability of the topological structure of a given class. The topology of the shape of the Fermi surfaces and the Dirac lines, as well as the interconnection of objects of different dimensionalities in momentum and frequency–momentum spaces, leads to the appearance of numerous classes of Lifshitz transitions.

The consequences of Lifshitz transitions are important in various areas of physics. In particular, the singular density of electronic states emerging at the transition is important for the construction of superconductors with an elevated transition temperature; the Lifshitz transition may be the reason for the origin of the small masses of elementary particles in our Universe; the black hole horizon serves as the surface of the Lifshitz transition between vacua with type-I and type-II Weyl points, etc.

Acknowledgments
This study was supported by the European Research Council (ERC) under the European Union's Horizon 2020 research and innovation programme (Grant Agreement No. 694248). The work on sections devoted to high-temperature superconductivity has been supported by RSCF (No. 16-42-01100).

References

1. Lifshits I M *Sov. Phys. JETP* **11** 1130 (1960); *Zh. Eksp. Teor. Fiz.* **38** 1569 (1960)
2. Hořava P *Phys. Rev. Lett.* **95** 016405 (2005)
3. Volovik G E *The Universe in a Helium Droplet* (Oxford: Clarendon Press, 2003)
4. Volovik G E *Lecture Notes Phys.* **718** 31 (2007)
5. Volovik G E *Low Temp. Phys.* **43** 47 (2017); *Fiz. Nizk. Temp.* **43** 57 (2017)
6. Zhang K, Volovik G E *JETP Lett.* **105** 519 (2017); *Pis'ma Zh. Eksp. Teor. Fiz.* **105** 504 (2017)
7. Volovik G E *JETP Lett.* **46** 98 (1987); *Pis'ma Zh. Eksp. Teor. Fiz.* **46** 81 (1987)
8. Dmitriev V V et al. *Phys. Rev. Lett.* **115** 165304 (2015)
9. Froggatt C D, Nielsen H B *Origin of Symmetry* (Singapore: World Scientific, 1991)
10. Volovik G E *JETP Lett.* **91** 55 (2010); *Pis'ma Zh. Eksp. Teor. Fiz.* **91** 61 (2010)
11. Sidharth B G et al. *Int. J. Mod. Phys. A* **31** 1630051 (2016)
12. Sidharth B G et al. *New Adv. Phys.* **10** 1 (2016)
13. Laperashvili L V, Nielsen H B, Das C R *Int. J. Mod. Phys. A* **31** 1650029 (2016)
14. Bennett D L, Nielsen H B, Froggatt C D, hep-ph/9710407
15. Volovik G E *JETP Lett.* **79** 101 (2004); *Pis'ma Zh. Eksp. Teor. Fiz.* **79** 131 (2004)
16. Volovik G E *Phys. Lett. A* **142** 282 (1989)
17. Liu W V, Wilczek F *Phys. Rev. Lett.* **90** 047002 (2003)
18. Barzykin V, Gor'kov L P *Phys. Rev. B* **76** 014509 (2007)
19. Agterberg D F, Brydon P M R, Timm C *Phys. Rev. Lett.* **118** 127001 (2017)
20. Timm C et al. *Phys. Rev.* **96** 094526 (2017)
21. Volovik G E *Sov. Phys. Usp.* **27** 363 (1984); *Usp. Fiz. Nauk* **143** 73 (1984)
22. Mäkinen J T et al., in *28th Intern. Conf. on Low Temperature Physics, LT28, 9–16 August 2017, Gothenburg, Sweden, Abstracts* (2017) Abst. 008; http://www.trippus.se/eventus/userfiles/84948.pdf
23. Vollhardt D, Maki K, Schopohl N *J. Low Temp. Phys.* **39** 79 (1980)
24. Zhu T et al. *Phys. Rev. Fluids* **1** 044502 (2016)
25. Voit J *Rep. Prog. Phys.* **58** 977 (1995)
26. Dzyaloshinskii I *Phys. Rev. B* **68** 085113 (2003)
27. Farid B, Tsvelik A M "Comment on "Breakdown of the Luttinger sum rule within the Mott–Hubbard insulator", by J. Kokalj and P. Prelovšek, Phys. Rev. B 78, 153103 (2008)"; arXiv:0909.2886; Kokalj J, Prelovšek P *Phys. Rev. B* **78** 153103 (2008); arXiv:0803.4468

28. Pracht U S et al. *Phys. Rev. B* **93** 100503(R) (2016)
29. Khodel' V A, Shaginyan V R *JETP Lett.* **51** 553 (1990); *Pis'ma Zh. Eksp. Teor. Fiz.* **51** 488 (1990)
30. Volovik G E *JETP Lett.* **53** 222 (1991); *Pis'ma Zh. Eksp. Teor. Fiz.* **53** 208 (1991)
31. Nozières P *J. Physique I* **2** 443 (1992)
32. Shashkin A A et al. *Phys. Rev. Lett.* **112** 186402 (2014)
33. Shashkin A A et al. *JETP Lett.* **102** 36 (2015); *Pis'ma Zh. Eksp. Teor. Fiz.* **102** 40 (2015)
34. Yudin D et al. *Phys. Rev. Lett.* **112** 070403 (2014)
35. Volovik G E *JETP Lett.* **59** 830 (1994); *Pis'ma Zh. Eksp. Teor. Fiz.* **59** 798 (1994)
36. Melnikov M Yu et al. *Sci. Rep.* **7** 14539 (2017)
37. Drozdov A P et al. *Nature* **525** 73 (2015)
38. Eremets M I, Drozdov A P *Phys. Usp.* **59** 1154 (2016); *Usp. Fiz. Nauk* **186** 1257 (2016)
39. Quan Y, Pickett W E *Phys. Rev. B* **93** 104526 (2016)
40. Bianconi A, Jarlborg T *Novel Supercond. Mater.* **1** 37 (2015)
41. Souza T X R, Marsiglio F *Int. J. Mod. Phys. B* **31** 1745003 (2017)
42. Shi X et al. *Nature Commun.* **8** 14988 (2017)
43. von Neumann J, Wigner E *Phys. Z.* **30** 467 (1929)
44. Volovik G E, Zubkov M A *Nucl. Phys. B* **881** 514 (2014)
45. Volovik G E, Konyshev V A *JETP Lett.* **47** 250 (1988); *Pis'ma Zh. Eksp. Teor. Fiz.* **47** 207 (1988)
46. Klinkhamer F R, Volovik G E *Int. J. Mod. Phys. A* **20** 2795 (2005)
47. Volovik G E, Gor'kov L P *Sov. Phys. JETP* **61** 843 (1985); *Zh. Eksp. Teor. Fiz.* **88** 1412 (1985)
48. Volovik G E *JETP Lett.* **105** 273 (2017); *Pis'ma Zh. Eksp. Teor. Fiz.* **105** 245 (2017)
49. Creutz M *JHEP* **2008** (04) 017 (2008)
50. Creutz M *Ann. Physics* **342** 21 (2014)
51. Nielsen H B, Ninomiya M *Nucl. Phys. B* **185** 20 (1981); *Nucl. Phys. B* **193** 173 (1981)
52. Soluyanov A A et al. *Nature* **527** 495 (2015)
53. Huhtala P, Volovik G E *JETP* **94** 853 (2002); *Zh. Eksp. Teor. Fiz.* **121** 995 (2002)
54. Li D et al. *Phys. Rev. B* **95** 094513 (2017)
55. Alidoust M, Halterman K, Zyuzin A A *Phys. Rev. B* **95** 155124 (2017)
56. Volovik G E *JETP Lett.* **104** 645 (2016); *Pis'ma Zh. Eksp. Teor. Fiz.* **104** 660 (2016)
57. Painlevé P *C.R. Acad. Sci.* **173** 677 (1921); Gullstrand A *Arkiv. Mat. Astron. Fys.* **16** (8) 1 (1922)
58. Unruh W G *Phys. Rev. Lett.* **46** 1351 (1981)
59. Unruh W G *Phys. Rev. D* **51** 2827 (1995)
60. Kraus P, Wilczek F *Mod. Phys. Lett. A* **9** 3713 (1994)
61. Nissinen J, Volovik G E *JETP Lett.* **105** 447 (2017); *Pis'ma Zh. Eksp. Teor. Fiz.* **105** 442 (2017)
62. Heikkilä T T, Volovik G E *New J. Phys.* **17** 093019 (2015)
63. Autti S et al. *Phys. Rev. Lett.* **117** 255301 (2016)
64. Mikitik G P, Sharlai Yu V *Phys. Rev. B* **73** 235112 (2006)
65. Mikitik G P, Sharlai Yu V *Low Temp. Phys.* **34** 794 (2008); *Fiz. Nizk. Temp.* **34** 1012 (2008)
66. Mikitik G P, Sharlai Yu V *Phys. Rev. B* **90** 155122 (2014)
67. Takane D et al. *Quantum Mater.* **3** 1 (2018)
68. Hyart T, Heikkilä T T *Phys. Rev. B* **93** 235147 (2016)
69. So H *Prog. Theor. Phys.* **74** 585 (1985)
70. Ishikawa K, Matsuyama T *Z. Phys. C* **33** 41 (1986)
71. Ishikawa K, Matsuyama T *Nucl. Phys. B* **280** 523 (1987)
72. Haldane F D M *Phys. Rev. Lett.* **61** 2015 (1988)
73. Volovik G E *Sov. Phys. JETP* **67** 1804 (1988); *Zh. Eksp. Teor. Fiz.* **94** (9) 123 (1988)
74. Kourtis S et al. *Phys. Rev. B* **96** 205117 (2017)
75. Rombouts S M A, Dukelsky J, Ortiz G *Phys. Rev. B* **82** 224510 (2010)